PHYSICAL REVIEW B **72**, 075323 (2005)

Nanoscale structures formed in silicon cleavage studied with large-scale electronic structure calculations: Surface reconstruction, steps, and bending

Takeo Hoshi,[1,2] Yusuke Iguchi,[1] and Takeo Fujiwara[1,2]
[1]*Department of Applied Physics, University of Tokyo, Bunkyo-ku, Tokyo, Japan*
[2]*Core Research for Evolutional Science and Technology (CREST),*
Japan Science and Technology Agency (JST), Kawaguchi-shi, Saitama, Japan
(Received 8 September 2004; revised manuscript received 16 March 2005; published 9 August 2005)

The 10-nm-scale structure formed in silicon cleavage is studied by the quantum mechanical calculations of large-scale electronic structure. The cleavage process was simulated and the results show not only the elementary process of the (experimentally observed) (111)-(2×1) surface reconstruction but also several step-formation processes. These processes are studied by analyzing electronic freedom and compared with scanning tunneling microscopy experiments. The stability mechanism of the (111)-(2×1) cleavage mode is presented beyond the traditional approach with surface energy. In other results, the cleavage path was bent into the experimentally observed planes, owing to the relative stability among cleavage modes. Several common aspects between cleavage and other phenomena are discussed from the viewpoints of nonequilibrium process and 10-nm-scale structure.

DOI: 10.1103/PhysRevB.72.075323 PACS number(s): 68.35.−p, 71.15.Pd, 62.20.Mk

I. INTRODUCTION

Cleavage is a nonequilibrium process and its dynamical mechanism is essential. In particular, the cleavage of silicon single crystals is of great interest from the multiscale viewpoint between macroscale and atomic-scale pictures. In the macroscale picture, silicon shows perfect brittleness and brittle fracture is usually described by continuum mechanics.[1–3] On the other hand, the cleaved surface shows atomic-scale reconstructions, which are observed by scanning tunneling microscopy[4] (STM) and other experiments. The multiscale feature, as discussed in this paper, appears in 10-nm-scale region near the crack tip, though such processes cannot be seen by direct (*in situ*) experimental observation.

A fundamental question is what Miller index and surface reconstruction appears at the cleavage surface. One may predict from the traditional viewpoint that the cleavage plane should be that with the smallest surface energy or the smallest energy loss with forming surface. This prediction, however, fails to explain the following experimental facts: (i) The easiest cleavage plane of Si is a metastable (111)-(2×1) structure[4–10] and will change, irreversibly, to the ground-state (7×7) structure.[4,11] (ii) The (110) cleavage plane is also experimentally observed but less favorable [see an experimental (STM) study,[12] and a recent theoretical study[13]]. (iii) The cleaved Ge(111) surface also shows the same (2×1) structure, while the ground-state surface structure is the c(2×8) structure.[4,14,15] These facts imply the importance of direct cleavage simulations with electronic structure. Although such simulations have been carried out thus far,[8,9,13] the system size is limited to the order of 10^2 atoms.

In this paper, the cleavage of silicon is studied with quantum mechanical calculations of large-scale electronic structures[16–21] and we use a transferable Hamiltonian[22] in the Slater-Koster (tight-binding) form. The methodology is reviewed briefly in Appendix A. The method realizes the cleavage process with more than 10^4 atoms or a sample length of 10 nm. This paper is organized as follows: Section II describes the important aspects discussed in this paper. The easiest cleavage mode on the (111)-(2×1) plane is discussed in Sec. III and Sec. IV. The latter section focuses on step formations. The simulation results for bending in the cleavage path are presented in Sec. V. Finally, in Sec. VI, several common aspects of nanoscale structures are discussed for cleavage and other phenomena.

II. ASPECTS OF CLEAVAGE IN REAL CRYSTAL

Several aspects of cleavage are pointed out as the foundation of the present theoretical study. The first one is the fact that cleavage, as a nonequilibrium process, has a typical time scale that is determined by the cleavage propagation velocity v_{prop}. In the continuum mechanics and many experiments, the propagation velocity v_{prop} is given on the order of, but less than, the sound velocity or the Rayleigh wave velocity ($v_{\mathrm{R}}=4.5$ km/s$=4.5$ nm/ps for Si).[2,3,23] When cleavage propagates by a typical atomic length scale, say $\Delta L \approx 1$ nm for Si, it accompanies elementary processes of bond breaking and surface reconstruction in the time scale of $\Delta T = \Delta L / v_{\mathrm{prop}}$ (less than 1 ps). Since the processes occur within this time scale, the reconstruction in cleavage should occur *locally*, unlike that in annealing. As a typical process, a surface-bound state tends to be formed between electrons in *nearest-neighbor* dangling-bond sites, as illustrated in Figs. 1(a)–1(c). This nearest-neighbor reconstruction mechanism will directly give the experimentally observed (2×1) reconstruction (see Sec. III).

The second aspect comes from crystal structure. Figure 1(d) shows the possible cleavage paths on the Si(111) plane, with or without step formation. Unlike the toy model of Figs. 1(a)–1(c), the system does not have the mirror symmetry with the cleavage plane and the upper and lower cleaved surfaces are inequivalent in symmetry. In particular, the in-

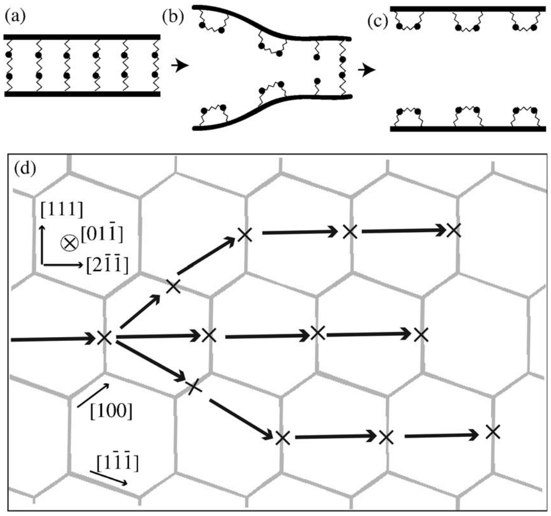

FIG. 1. (a)–(c) Toy model of cleavage, in which surface reconstruction is illustrated as dimerization. (d) Possible cleavage paths on Si(111) plane.

equivalence between the upper and lower stepped paths in Fig. 1(d) is distinctive in experiments.

Since experiments reported only the (111) or (110) cleavage plane, theory should explain why other surfaces *do not* appear. An interesting fact is that the calculated surface energy of the reconstructed (001) surface is *smaller* than that of the (111)-(2×1) surface $(\gamma^{4\times2}_{(001)}=1.41\ \mathrm{J/m^2}<\gamma^{2\times1}_{(111)}=1.44\ \mathrm{J/m^2})$.[14,24] Therefore, the absence of the (001) cleavage surface is not simply predicted by surface energy.[25] The possibility of the (001) cleavage mode was investigated in our previous study,[18] in which the (001) cleavage planes are observed for small sample sizes less than 10 nm. For larger sizes, the flat (001) cleavage surface becomes fairly unstable and many steps form. The instability of the (001) cleavage mode is helpful in understanding the stability of the (111) cleavage mode, as discussed in Sec. IV.

III. (111)-(2×1) CLEAVAGE MODE

The easiest cleavage mode in experiments is that with Si(111)-(2×1) surface. Pandey's π-bonded structure[5] is now widely accepted as the atomic structure of the cleaved surface.[4,6–10] A surface formation process was shown in a simulation,[8] when a *parallel* separation is introduced in a slab with the minimal periodic simulation cell for the (2×1) structure (see Figs. 1 and 2 of Ref. 8).

The present cleavage simulations are performed with the $[2\bar{1}\bar{1}]$ propagation directions [Fig. 1(d) for geometry], which are consistent with typical experiments (see Fig. 1 of Ref. 26, for example). An external load is imposed and its physical origin is the concentrated elastic field in the macroscale experimental sample. See Appendix B for details. A smaller sample with 416 atoms was also simulated, as shown in Appendix C, so as to confirm the quantitative agreement with previous experimental or theoretical studies. In all cases, the periodic boundary condition is imposed in the $[01\bar{1}]$ direction, which is orthogonal to the cleavage propagation direction. The periodic length contains eight atomic layers or is four times larger than that of the minimum crystalline periodicity. In some simulations, the atomic motion is under a constraint by the minimum crystalline periodicity in the $[01\bar{1}]$ direction. We call this constraint, the two-dimension-like or "2D-like constraint." For a systematic investigation, simulations were carried out with and without the 2D-like constraint.

Figure 2 shows an example of the simulation within the 2D-like constraint, in which a step appears. The sample contains 11 096 atoms. Hereafter, the bonds (rods) are drawn just as a guide for eye. From Fig. 2, the cleavage propagation velocity is estimated to be $v_{\mathrm{prop}}\approx 2\ \mathrm{nm/ps}=2\ \mathrm{km/s}$, as expected in Sec. II. The cleaved surface in Fig. 2(f) contains the π-bonded (111)-(2×1) structure, of which unit structure is a set of seven-membered and five-membered rings.

A. Elementary reconstruction process

Figures 3(a)–3(d) show a process of the (2×1) reconstruction. As in the previous simulation with parallel separation,[8] the reconstruction process has two stages: The buckled (2×1) structure of Fig. 3(e) appears, as shown in Fig. 3(b), when the two dangling-bond electrons at the *C* and *D* sites form an atomic (lone-pair) state at the *D* site.[27] After that, the π-bonded (2×1) structure of Fig. 3(f) appears, since (i) the atomic state at the *D* site is transformed into the π-bonding state between the *B* and *D* sites and (ii) the bond-

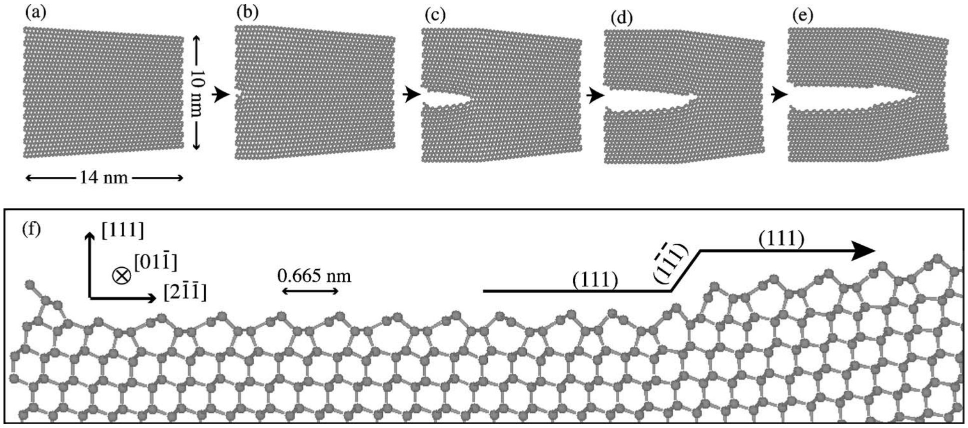

FIG. 2. Cleavage process of silicon with (111)-(2×1) cleaved surface. (a)–(e) Successive snapshots with a time interval of approximately 2 ps. (f) A part of the lower cleavage surface shown in the snapshot (e). A step is found and is classified into the $[\bar{2}11]$-type or via-$(1\bar{1}\bar{1})$-plane type that can be decomposed into the successive bending of cleavage planes as $(111)\rightarrow(1\bar{1}\bar{1})\rightarrow(111)$.

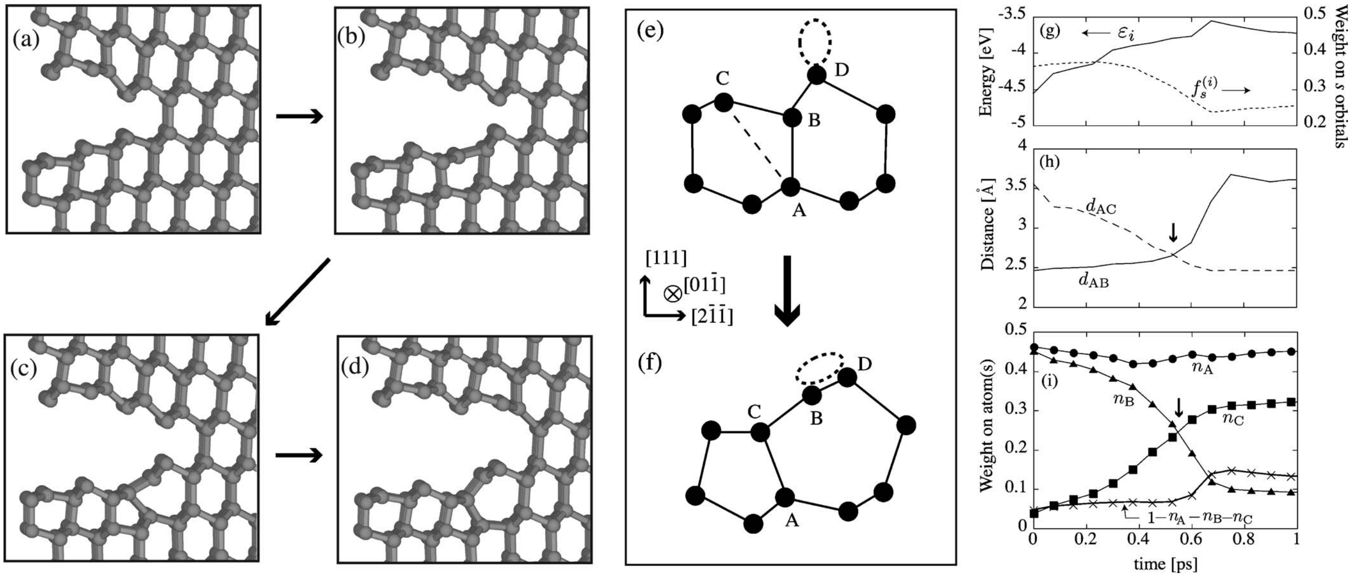

FIG. 3. (a)–(d) Initiation of cleavage while forming the (111)-(2×1) structure. (e), and (f) Schematic figures of the transition from (e) the buckled (2×1) structure to (f) the (tilted) π-bonded (2×1) structure. The former structure appears on the lower cleaved surface in (b) and the latter appears in (d). The oval in (e) indicates the presence of a lone pair state on the D atom site. The oval in (f) indicates the π-bonding zigzag chain in the direction perpendicular to the page. (g)–(i) Quantum mechanical analysis of a process in which the bonding wave function (ϕ_i) between A and B sites changes into that between A and C sites: (g) the one-electron energy $\varepsilon_i \equiv \langle \phi_i | H | \phi_i \rangle$ and the weight of s orbitals $f_s^{(i)}$ for the wave function ϕ_i; (h) the atomic distance between A and B sites (d_{AB}) and that between A and C sites (d_{AC}); (i) the spatial weight distribution on the A, B, and C atom sites ($n_{\rm A}, n_{\rm B}, n_{\rm C}$) for the wave function ϕ_i. The rest of the weight ($1-n_{\rm A}-n_{\rm B}-n_{\rm C}$) is also plotted.

ing state between the A and B sites is transformed into one between the A and C sites, so as to reproduce the tetrahedral coordination in the C site. In the three-dimensional view, a π-bonding zigzag chain appears in the direction perpendicular to the page. Hereafter, the transition from the buckled structure into the π-bonded one is called the "BP transition." Note that the resultant π-bonded structures are always tilted, since the D or B site is shifted to the vacuum side. The two tilted structures are inequivalent in symmetry and have a small difference in surface energy.[10,14] In this paper, however, we do not focus on the difference between the two tilted structures.

The above process of (ii) is monitored by the following quantum mechanical analysis: Figure 3(g) shows the one-electron energy $\varepsilon_i \equiv \langle \phi_i | H | \phi_i \rangle$ and the weight of s orbitals $f_s^{(i)}$.[18] For example, $f_{\rm s}^{(i)} = 1/4$ in an ideal sp^3 hybridized state. Figure 3(h) shows the distances between A, B, and C sites. Figure 3(i) shows the spatial weight distribution ($|\phi_i(\boldsymbol{r})|^2$) on atom sites. The intermediate wave function, indicated as the arrow in Fig. 3(h) or 3(i), shows no characteristic feature in ε_i and $f_s^{(i)}$, such as maxima, minima or plateaus. This is quite different from the reconstruction process on the (001) surface,[18] in which the intermediate wave function shows a plateau with a large weight on the s orbitals ($f_s^{(i)} \approx 0.8$).

B. Role of anisotropic surface strains

We studied the role of anisotropic surface strains in the process of the BP transition. Figure 4(a) demonstrates the presence of an anisotropic strain force on (111) surface with coexistence of the buckled and π-bonded (2×1) structures. The anisotropic strain force, depicted by an arrow in Fig. 4(a), enhances a further BP transition of the next left unit. Owing to the crystalline symmetry, the strain force on the upper and lower cleaved surfaces shows the opposite direction to each other, as shown by solid arrows in Fig. 4(b). This explains that the π-bonded structure appears on the lower cleavage surface in Fig. 3(d), but not on the upper one. Since the experiments support the π-bonded structure,[6,10] the π-bonded structure should appear commonly on the upper and lower surfaces. Such a result is obtained in Fig. 4(c), in which an additional constant force is imposed in the left direction on several leftmost atoms of the upper cleaved surface. The origin of the additional force is the fact that the simulation sample should be *embedded* in a macroscale sample. In the embedded situation, the boundary region of the simulation sample should be connected with a macroscale region of π-bonded (2×1) structures, which causes the stain force on surface atoms near the boundary of the simulation sample. The strength of the additional force f can be characterized by the energy quantity $E_f \equiv f \Delta l$ with the typical length scale of atomic distance $\Delta l \equiv 1$ Å. In the present case, the order of E_f is 1 eV. This energy cost is not only that for motivating the surface reconstruction but also for introducing large deformation on the deeper (subsurface) layers near the left sample (boundary) surface.

We also found that the sample geometry can have an effect on the possible BP transition through strain. For example, the BP transition seems to occur more easily in a *thicker* sample, with a larger sample length in the [111] direction, since the BP transition should accompany the strain in deeper (subsurface) layers. This observation was unchanged, when additional simulations were carried out by

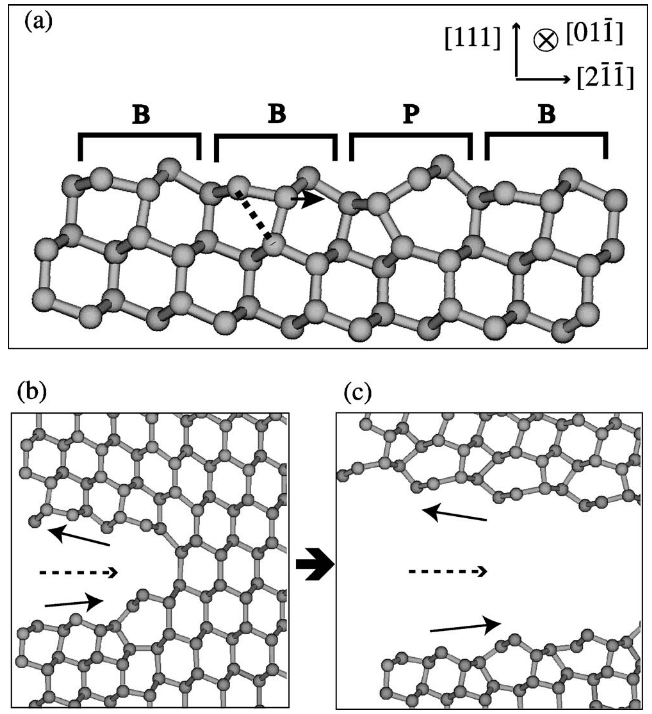

FIG. 4. (a) Si(111) surface with coexistence of the buckled and π-bonded (2×1) structures. The induced strain is shown as an arrow at the boundary between the buckled and π-bonded structures. The dashed line indicates the bond site that will appear after the next induced BP transition. (b) and (c) Two snapshots of cleavage process. The solid arrow corresponds to the direction of the possible surface strain force shown in (a). The dashed arrow denotes the cleavage propagation direction.

more complicated Hamiltonians with a better reproduction of surface energy. A more systematic investigation should be carried out, in the future, on the quantitative condition of the BP transition.

IV. STEP FORMATION IN CLEAVAGE

Several (111) cleavage simulations contain step formation. There are two inequivalent paths shown as the upper and lower paths in Fig. 1(d). The "upper" type of path is usually called the "$[\bar{2}11]$ type," since the step is *descending* in the $[\bar{2}11]$ direction. In the same manner, the "lower" type is called the "$[2\bar{1}\bar{1}]$ type." The two types of step are experimentally reported. In early papers,[4,11,28] it was reported that the *lower* path in Fig. 1(d), the $[2\bar{1}\bar{1}]$ type is predominant. In later experimental papers,[29] however, the *upper* path, i.e., the $[\bar{2}11]$ type step, was reported. In our simulations, both types of step are observed.

A. Upper-type step

First, we discuss the step in Fig. 2, which is classified into the upper path in Fig. 1(d) or the $[\bar{2}11]$ type. This type of step was observed with and without the 2D-like constraint. The formation process is shown in Fig. 5. Hereafter, the members of several rings are plotted, such as 6, 5, or 7, so as to clarify the reconstruction. This step can be decomposed into the successive bendings in the cleavage path as $(111)\rightarrow(1\bar{1}\bar{1})\rightarrow(111)$ planes [See Fig. 1(d) and Fig. 2]. That is, the step is formed *through* the $(1\bar{1}\bar{1})$ plane and we call the step, the "via-$(1\bar{1}\bar{1})$-plane" type. In the crystalline geometry, the (111) and $(1\bar{1}\bar{1})$ planes are equivalent. If we ignore the reconstruction (or quantum mechanical) freedom, the step formation can be understood, since bending between equivalent planes can occur by the local fluctuation of the (concentrated) elastic field at the crack tip, particularly in its angular dependence.

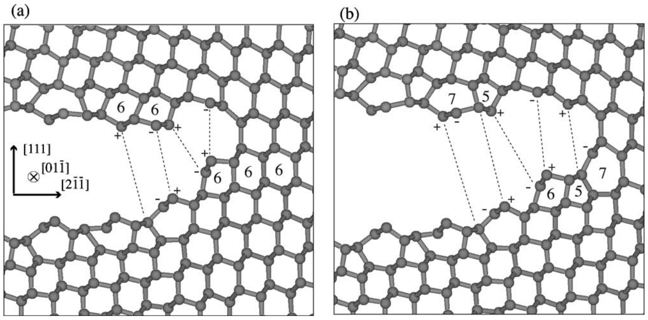

FIG. 5. Step formation process on (111) cleavage plane. The step is classified into the $[\bar{2}11]$-type or via-$(1\bar{1}\bar{1})$-plane-type step [see Fig. 2(f)]. Two snapshots with a time interval of approximately 0.6 ps are shown. The dashed lines indicate the initial (crystalline) bonds. The $+$ and $-$ symbols on atoms indicate excess and deficit electron populations, respectively.

As a quantum-mechanical analysis, snapshots of the step formation are shown in Fig. 5, in which atoms with excess and deficit electron populations are marked $+$ and $-$, respectively. The initial bonding states (dashed line) changed into the surface-bound state mainly localized on a $+$ atom site. A $+$ atom site is always placed at the vacuum side of a buckled structure, which can be understood by the general quantum-mechanical tendency.[30] The resultant surface shows a balanced structure with the alternate alignment of $+$ and $-$ sites. The present step structure is concluded to be a possible one, although it has not yet been confirmed experimentally.

Now we comment on a pioneering theoretical paper, by Chadi and Chelikowsky,[31] in which the upper and lower types of steps are compared with assumed atomic structures. They concluded that the *upper* path is unrealistic, which seems to be in contrast to the present result. The contrast appears, because the present step structure is different from that assumed in Ref. 31. In this reference, the dangling bonds at the step edge are assumed to be rebonded with each other in *the perpendicular direction* of the page of Fig. 1(d), but such a rebonding process results in only a tiny energy gain. In the present step structure of Fig. 5, on the other hand, the dangling bond electrons at the step edge are rebonded *within the plane* of Fig. 1(d), whose energy gain mechanism is explained above.

B. Lower-type step

Several simulations result in the appearance of the other type of step, the *lower-type* step in Fig. 1(d) or the $[2\bar{1}\bar{1}]$

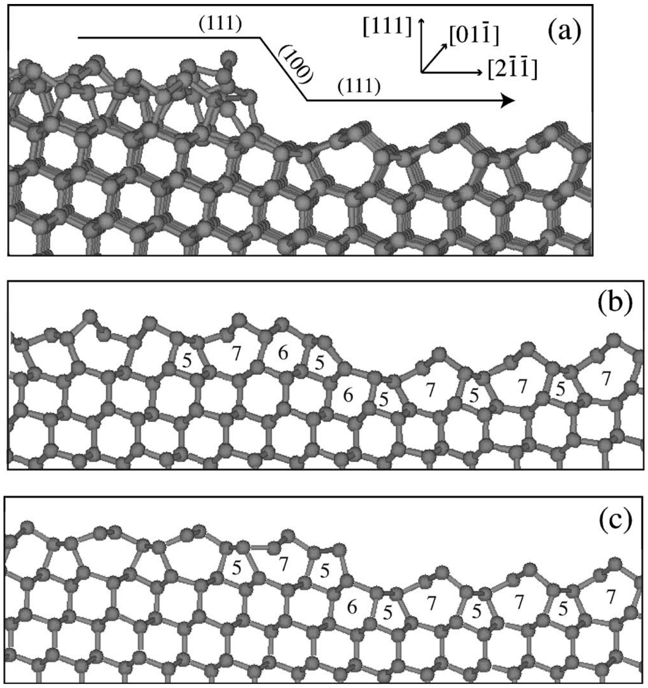

FIG. 6. (a) (111) cleaved surface with $[2\bar{1}\bar{1}]$-type or via-(100)-plane-type step. The arrow indicates the cleavage propagation direction. (b), (c): Two "slices" of (a) (see text for details).

type, when they were carried out without the 2D-like constraint or minimal periodicity in the $[01\bar{1}]$ direction. An example is shown in Fig. 6(a). To observe the freedom in the $[01\bar{1}]$ direction, we classify the atoms, by their initial positions, into subsystems or "slices." Each slice contains atoms within the minimum unit length (two atom layers) in the $[01\bar{1}]$ direction. Four slices are defined in Fig. 6(a) and two of them are shown in Figs. 6(b) and 6(c).

In Fig. 6(a), the cleaved surface is defective before the step formation. In the defective area of Figs. 6(b) and 6(c), six-membered rings appear in the surface layer, as well as five-membered or seven-membered rings. A defective area also appears in flat (nonstepped) areas, as in Fig. 7. The appearance of the defective six-membered rings means that the reconstruction of the dangling-bond electrons does not occur *within the slice*. We should recall that an ideal (111) surface has symmetry with a $\pm 2\pi/3$ rotation and the (2×1) reconstruction mechanism shown in Fig. 3(e) or 3(f) is possible in the $[2\bar{1}\bar{1}]$, $[\bar{1}2\bar{1}]$, and $[\bar{1}\bar{1}2]$ directions.

This type of step formation is decomposed into the successive bendings of cleavage as $(111)\rightarrow(100)\rightarrow(111)$ planes. In other words, the step is formed *through* the (100) plane and we call the step the "via-(100)-plane" type [see Fig. 1(d) for geometry]. At the step edge, the dangling bond sites are equivalent to those on a (100) or (001) plane. The reconstruction among them is possible with an energy gain of dimerization.[31] The actual process of successive bond breakings and reconstructions on (100) surface can be obtained as an unstable cleavage mode.[18] With the 2D-like constraint, however, the dimerization is prohibited. This is why this type of step does *not* appear within the 2D-like constraint.

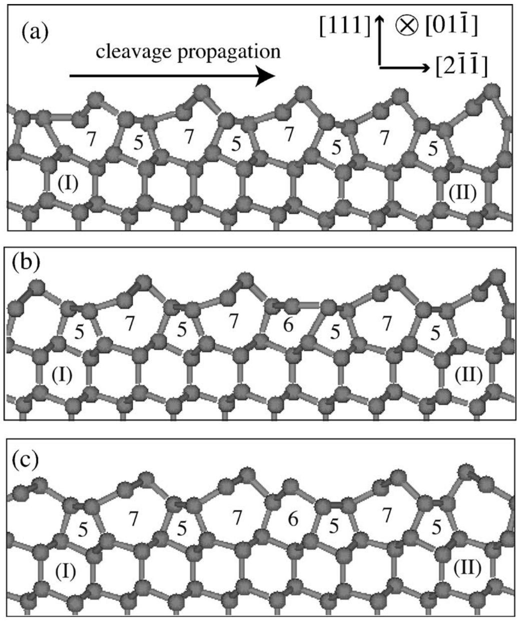

FIG. 7. Defective area on cleaved Si(111) surface. Three slices are picked out. The six-membered rings marked (I) and (II) are geometrically equivalent among slices (a)–(c).

The geometries in Fig. 6 can be compared with those proposed in STM experiments.[28] The geometry of Fig. 6(b) is identical to that of Fig. 5(b) in Ref. 28, because of the same alignment of the ring structures: $5\rightarrow 7\rightarrow 6\rightarrow 5$ before the step and $6\rightarrow 5\rightarrow 7$ after the step. In the same manner, the geometry of Fig. 6(c) is identical to that of Fig. 5(a) in Ref. 28 only before the step ($5\rightarrow 7\rightarrow 5$). After the step, however, the present geometry ($6\rightarrow 5\rightarrow 7$) is different, by one six-membered ring, from that shown in Ref. 28 ($6\rightarrow 6\rightarrow 5\rightarrow 7$).

The present investigation does *not* show that the upper type or lower type of step in Fig. 1(d) is more favorable than the other, because the present simulations were carried out under the periodic boundary conditions in the $[01\bar{1}]$ direction. We speculate that the appearance of the upper path, the $[\bar{2}11]$-type step, should be enhanced, because the step can be formed within the minimal crystalline periodicity in the $[01\bar{1}]$ direction. We have been informed that the two types of step are observed in STM images[32] and we consider that a more systematic investigation is desirable both theoretically and experimentally.

C. Step formation and stability of cleavage mode

The present study of step formation can lead to the stability mechanisms of the (111)-(2×1) cleavage mode, since a stable cleavage mode should be *robust* against possible disorders and fluctuations. We have discussed that a step formation is decomposed into successive bendings of the cleavage plane, such as $(111)\rightarrow(100)\rightarrow(111)$ planes. The former and latter bending processes correspond to the deviation and (quick) recovery of the (111) cleavage mode, respectively. Since the π-bonded (2×1) structure has a π-bonded zigzag

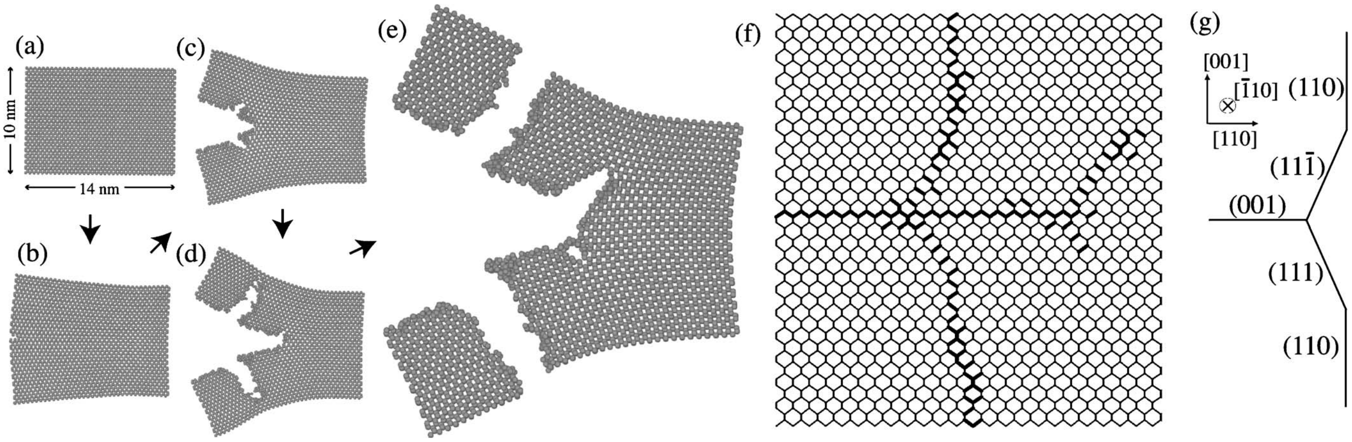

FIG. 8. Cleavage process of silicon with bending of cleavage planes. (a)–(e) Snapshots with a time interval of approximately 1 ps. Atoms are drawn as balls from the viewpoint of the $[\bar{1}10]$ direction. (f) The broken bond sites in snapshot (e) are plotted as bold lines in the ideal (crystalline) geometry. (g) Indices of geometry in (f).

chain perpendicular to the cleavage propagation direction, it can accompany the ordering in the surface structure. Actually, in Fig. 6, the step formation changes the cleaved surface from a disordered (defective) structure into an ordered (2×1) structure.

Another stability mechanism can be found in the possibility of multiple propagation directions. When the (2×1) structures on the (111) and (001) surfaces are compared, a crucial difference comes from symmetry. In the limited growth of the (001) cleavage mode,[18] the cleavage propagates easily in the dimerization direction. The axis of the dimerization direction is unique on the (001) surface and a (single) step formation changes the axis perpendicularly $[(2\times1)\rightarrow(1\times2)]$. As a consequence, a cleavage growth with multiple propagation directions requires step formation and the resultant (001) cleaved surfaces tend to be *rough* with many steps.[18] The steps on the (111) surface, on the other hand, can preserve the cleavage propagation direction or the direction of the π-bonded chain $[(2\times1)\rightarrow(2\times1)]$, as shown in this section. Moreover, the ideal (111) surface, unlike the (001) surface, has three equivalent axes of stable cleavage propagation: the $[2\bar{1}\bar{1}]$, $[\bar{1}2\bar{1}]$, and $[\bar{1}\bar{1}2]$ axes. In conclusion, the stability of the (111) cleavage mode is supported by the geometrical features: (i) A step can be formed without changing the cleavage propagation direction. (ii) The cleavage propagation direction can be changed without step formation. The above feature (ii) should result in multiple domains without step formation. Actually, an experimental STM image, Fig. 2 in Ref. 26, shows a cleaved (111) surface with multiple domains. We speculate that such a multiple domain structure is formed, because the cleavage propagation directions are locally different.

We should emphasize that the present stability mechanisms, the robustness against step formation and the possible growth with multiple propagation directions, cannot be explained by traditional discussion on surface energy.

V. BENDING IN CLEAVAGE PATH

Finally, the preference of the (111) or (110) surface in cleavage experiments is presented by simulation. We expect that, even if the simulation initiates the cleavage on other planes, the cleavage path will be bent into a more favorable plane. The above was confirmed by simulations. Hereafter, symmetrically equivalent planes are called by their type. For example, $(1\bar{1}\bar{1})$ and $(11\bar{1})$ planes are (111)-type planes.

An example is shown in Figs. 8(a)–8(e). The sample contains 10 368 atoms and the sample size is 10 nm × 14 nm on the $(\bar{1}10)$ plane. The periodic boundary is imposed in the $[\bar{1}10]$ direction by eight atomic layers. We prepare an initial "seed" of cleavage on the (001) plane. An external force acts on the atoms near the sample surfaces except the left one. See Appendix B for details.

Figure 8(f) shows the broken-bond sites on the crystalline geometry and the corresponding indices are drawn in Fig. 8(g). In this case, the bendings are observed from the initial (001) plane to (111)-type and/or(110)-type planes, such as $(001)\rightarrow(11\bar{1})\rightarrow(110)$ planes. Here, the (110)-type planes appear only near the sample surface, which implies that the appearance of (110)-type planes is enhanced by the present sample geometry. Different paths were observed under different simulation conditions, such as tuning the magnitude of the external load, preparing a different sample geometry, changing the region of imposing external force, and setting a different cleavage seed. For example, we observed a bending between two (111)-type planes, such as $(111)\rightarrow(\bar{1}11)$ planes. In conclusion, a (111)-type or (110)-type plane appears, while no (001)-type plane appears except the initially prepared one. This conclusion is consistent with the experimental preference of the (111)-type and (110)-type cleaved surfaces.

Bending in the cleavage path can recover the ordering in cleaved surface. We observed sometimes that the cleavage path is bent from a disordered (defective) surface (before bending) into an ordered surface with a well-defined reconstruction (after bending). In Fig. 9(a), the area after bending contains the buckled (110) surface structure, known for a typical reconstruction.[14] In the process shown in Figs. 9(b) and 9(c), the resultant (111) cleavage plane contains the π-bonded (111)-(2×1) structure.

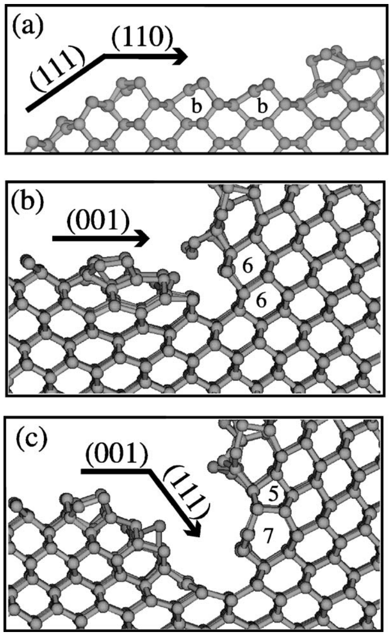

FIG. 9. Appearance of well-defined reconstructed surfaces after bending in cleavage path. The figures are drawn by projection from the $[\bar{1}10]$ direction. (a) Bending from the (111) plane to (110) plane. After the bending, the buckled (110) surface structures appears, as indicated by b. (b) and (c) Two snapshots of the bending from (001) plane to (111) plane. The resultant (111) plane contains the π-bonded (2×1) structure with seven-membered and five-membered rings, indicated as 7 and 5 in (c).

VI. GENERAL DISCUSSION

From the viewpoints of (i) the nonequilibrium process and (ii) the 10-nm-scale structure, several common aspects can be found between the present result of cleavage and other phenomena. From the viewpoint of the nonequilibrium process (i), as discussed in Sec. II, the metastable Si(111)-(2×1) structure appears, owing to the local reconstruction mechanism within a limited time scale. Since the mechanism is general in the quantum-mechanical picture, we expect the (111)-(2×1) surface also in other nonequilibrium processes. Actually, we were informed that the corresponding STM image is found in a Si(111)$\sqrt{3}\times\sqrt{3}$-Ga surface, when the Ga atoms are locally removed at room temperature.[33] At higher temperatures, the (7×7) structure appears.[34] The above situation is another "fast" process almost free from thermal equilibration. A review article[4] lists other experiments with the appearance of the Si(111)-(2×1) structure.

From the viewpoint of the 10-nm-scale structure (ii), the energy competition between volume and surface terms is essential. The volume term is dominant in the macroscale system and dimensional analysis shows a crossover of mechanical property between nanoscale and macroscale systems. In the case of silicon, the energy competition originates from that between the sp^3 (bulk) term and the non-sp^3 (surface) term. We speculate that the length scale of the crossover is universal in silicon, because the surface energy is always on the same order among different surface indices.[24] The crossover at 10 nm scale is found in the present result, because the step formation or the bent cleavage path appears only in the samples larger than 10 nm. The crossover may be seen also in the size dependence of the shape in self-organized Si islands.[35] Islands with a size of 10 nm or less have a semispherical shape and those with a larger size have a pyramidal shape with facets in well-defined indices. These crossovers can be understood, because a well-defined reconstructed surface appears only when the system size is much larger than the unit length of the reconstructed surface (~ 1 nm).

The present method of large-scale electronic structure calculation has wide applications and is not specific to cleavage. The structural property at 10 nm scale is an urgent problem of the present technology and can be a future study of the present method.

ACKNOWLEDGEMENTS

We thank Yutaka Mera, Kouji Maeda, and Masakazu Ichikawa (University of Tokyo) for discussion on experiments. Numerical calculation was partly carried out using the facilities of the Japan Atomic Energy Research Institute and the Institute for Solid State Physics, University of Tokyo. This work is financially supported by "Research and Development for Applying Advanced Computational Science and Technology" of the Japan Science and Technology Corporation.

APPENDIX A: METHODS FOR LARGE-SCALE ELECTRONIC STRUCTURE CALCULATION

In recent years, we have developed theories and program codes for large-scale electronic structure calculations.[16–21] Among them, a variational (VR) procedure for generalized Wannier states[16,21] is used in the present cleavage simulations. The Wannier state is well-defined localized "chemical" wave function in condensed matter, such as a bonding state or a lone-pair state, with a slight spatial extension. The suffix i of a Wannier state ϕ_i denotes its localization center. A bench mark is shown in the left panel of Fig. 10, in which our calculations are compared with the conventional method for calculating eigenstates. The figure shows not only the result of the VR procedure but also that of another Wannier state method called the "perturbative (PT) procedure."[16,18] The circle and square indicate the results of the conventional method and PT procedure, respectively, by a standard workstation.[18] The triangle and cross indicate the results of the VR procedure with 32 CPUs and PT procedure with 512 CPUs, respectively, by a parallel computation system (SGI Origin 3800™). The parallelism is carried out by the OpenMP technique (www.openmp.org). All the results of our methods are "order-N," or linearly proportional to the system size (N). The PT procedure is much faster than the VR procedure but its applicability is strictly limited.[16,18] Several related methods[36] were also developed but are not used in this paper.

Another methodological foundation is the transferable Hamiltonian[22] in the Slater-Koster (tight-binding) form, applicable to various circumstances, e.g., crystals, liquids, defects, and surfaces. Its success is based on the universality of

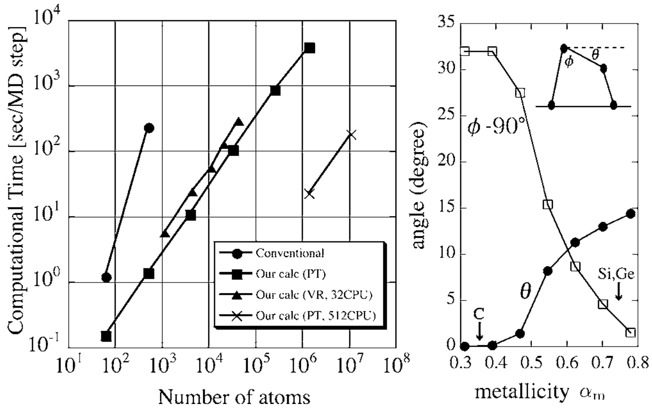

FIG. 10. (Left) Computational time for molecular dynamics simulation with up to 11 315 021 Si atoms. Our calculations are compared with the conventional calculation for the eigenstates. See text for explanations. (Right) Dimer geometry on (001) surface of group IV elements (C, Si, and Ge). The angle θ is the tilt angle and ϕ is the angle between the surface dimer and the plane that contains the two back bonds of the upper atom.

electronic structures, which has been known for decades[37–39] and can be founded by the *ab initio* theory.[40–42] Consequently, group IV elements can be systematically described by a one-parameter energy scaling theory.[16,17,37,38] The scaling parameter, "metallicity" α_{m}, is defined as

$$\alpha_{\mathrm{m}} \equiv \frac{\varepsilon_p - \varepsilon_s}{2t_{sp^3}}. \tag{A1}$$

Here, $(\varepsilon_p - \varepsilon_s)$ is the energy difference between the p and s orbitals and t_{sp^3} is the transfer energy along a bulk (sp^3) bond ($t_{sp^3} \equiv |V_{ss\sigma} - 2\sqrt{3}V_{sp\sigma} - 3V_{pp\sigma}|/4$). A typical value for C is $\alpha_{\mathrm{m}}=0.35$.[43] The values for Si and Ge are similar, $\alpha_{\mathrm{m}}=0.75-0.78$ (see Refs. 16 and 17 and references therein).

Several surface structures among C, Si, and Ge are systematically explained by the energy scaling theory. An example is shown in the dimer geometry on (001) surfaces. *Ab initio* calculations result in a *symmetric* dimer in the C case and similar *asymmetric* dimers in the Si and Ge cases (see Fig. 2 of Ref. 44, for example). In the right panel of Fig. 10, the above trend is reproduced with the present Hamiltonian by tuning the value of α_{m} or $(\varepsilon_p - \varepsilon_s)$. Since the (111)-(2 × 1) cleaved surface is commonly seen in Si and Ge,[15] the phenomena should hold a common mechanism in the present context of universality.

For validation of the present study, surface energy of silicon was calculated by the present Hamiltonian. The results are listed below with *ab initio* values[14] inside the parentheses: $\gamma_{001}^{4\times2}=1.58(1.41)$ J/m^2, $\gamma_{111}^{2\times1}=1.97(1.44)$ J/m^2, and $\gamma_{110}^{\mathrm{buckled}}=2.11(1.70)$ J/m^2, for the (001)-c(4 × 2) structure, the π-bonded (111)-(2 × 1) structure, and the buckled (110) structure, respectively. The present results reproduce the *ab initio* ones satisfactorily, particularly, the order of magnitude ($\gamma_{001}^{4\times2} < \gamma_{111}^{2\times1} < \gamma_{110}^{\mathrm{buckled}}$), though the absolute values are somewhat overestimated. Calculated surface energy of (001) surfaces with different reconstructions also gives satisfactory results.[45]

APPENDIX B: CONDITIONS OF CLEAVAGE SIMULATION

This appendix explains the technical conditions for cleavage simulation. The time step of the molecular dynamics was set at 3 fs. The center of gravity of the sample was fixed as a constraint. Sample surfaces were terminated by orientationally fixed sp^3 bonding states. This termination technique corresponds to the situation in which the sample is embedded in a bulk (sp^3-bonded) system. This situation is quite different from that with usual hydrogen termination, in which the atomic structure is deformed significantly from the tetrahedral geometry, owing to the large deviation from the sp^3 bonding.

Initial defect bonds were prepared for the cleavage "seed," which can be seen in Fig. 2(b) or Fig. 8(b). Actually, an additional short-range repulsive force was imposed on the atom pairs of selected bond sites. The number of the selected bond sites were, typically, two or three. Since the repulsive force is of short range, it will act on nothing after the bond breaking.

Cleavage was simulated with various ways of imposing external load on outer atoms of the simulation sample, which corresponds to the boundary condition of the sample.[21] If the sample is sufficiently large, the cleavage phenomena will be determined by the intrinsic nature of system, not by the boundary condition. The discussion in this paper is based on the results that are *not* sensitive to the boundary condition. We pick out the cases of Figs. 2 and 8 to explain the way of imposing external load. In Fig. 2, the external load is realized by the constrained movement. The atoms of the outermost two layers on the top and bottom sample surfaces were constrained under artificial movement in the [111] direction. Since the cleavage propagation velocity is on the order of the Rayleigh wave velocity $v_{\mathrm{R}}=4.5$ nm/ps, the velocity of the artificial movement should be much slower than v_{R}. If not, the atoms in the constraint motion (the atoms near the sample surfaces) are removed from the sample and no internal (cleavage) surface appears. In the case of Fig. 2, we chose $v_0=0.16$ nm/ps, as a typical value. In our simulations, the artificial movement was required to avoid forming multiple cleavage planes. The details are described elsewhere.[21] Within the above requirements for the artificial movement, the conclusions of the present paper are not changed. The way of controlling the artificial movement is reflected on the shape of the sample boundary in Figs. 2(a)–2(e).

Now we explain the case of Fig. 8, in which an external force field is imposed on selected atomic layers near the sample surfaces, except the left one. The thickness of the selected layers is 5 or 10% of the sample length. The force field is given as

$$\boldsymbol{F}(\boldsymbol{r}) = \frac{Kd_0^2}{\sqrt{2\pi r}}\frac{\boldsymbol{r}}{|\boldsymbol{r}|} \tag{B1}$$

with the relative coordinate $\mathbf{r}$ from the force center. The (two-dimensional) coordinate $\mathbf{r}$ is given on the $(01\bar{1})$ plane (see Fig. 1). The force center ($\boldsymbol{r}=0$) is fixed at the position of the initial defect and is placed almost at the middle of the left sample surface. The length d_0 is determined so that the volume per atom is given as d_0^3 ($d_0 \approx 3$ Å). The force field is consistent with the concentrated stress field given by the continuum mechanics of cleavage,[3] when its angular dependence is ignored. The angular dependence was ignored in our simulations, because it is defined only for a planar crack and is not valid in the stepped or bent cleavage paths discussed in this paper. In Fig. 8, K was set at $K=0.8$ MPa $\sqrt{m}$, which is slightly larger than the critical value ($K_{\mathrm{prop}}=0.7$ MPa $\sqrt{m}$) estimated in Appendix C. In several other simulations, the field center was under artificial movement, because the crack tip should move with the cleavage propagation. We did not find, however, a systematic difference in the resultant cleavage behavior.

Finally, in Figs. 2 and 8, the total kinetic energy was controlled by the thermostat method[46] with a typical temperature parameter of $T=800$ K. The temperature parameter T, however, does *not* correspond to the experimental temperature, since the simulation is a nonequilibrium process. In Fig. 2, for example, the constraint movement is introduced to the sample surfaces with the characteristic velocity v_0. The temperature parameter T should be sufficiently large to propagate the introduced deformation into the internal region.

APPENDIX C: ESTIMATION OF CRITICAL STRESS INTENSITY FACTOR

The critical stress intensity factor for cleavage propagation, K_{prop}, was estimated for the (111)-(2×1) cleavage mode with a smaller sample of 416 atoms. In the continuum theory with linear elasticity,[3] the divergent stress field is presented at the crack tip. When the center of the divergent field $\boldsymbol{R}_{\mathrm{c}}$ is given, the stress intensity factor K is introduced as the amplitude of the divergent field. Its critical value K_{prop} is a measurement of the critical external load and was determined in several experimental techniques and in the electronic structure calculations with hundreds of atoms.[9,13]

The present estimation of the critical factor K_{prop} was carried out within the following quasistatic picture: when the field center $\boldsymbol{R}_{\mathrm{c}}$ is shifted by one atomic increment, the crack tip should be shifted, also by one atomic increment, with the elementary bond-breaking and reconstruction process. If the factor K is not sufficiently large ($K<K_{\mathrm{prop}}$), however, the crack tip is not shifted. In practical simulations, the field center $\boldsymbol{R}_{\mathrm{c}}$ was chosen in the middle of a bond layer, which is shown as the nonstepped path of Fig. 1(d). As constraints, outer atoms were fixed with the linear elastic displacement of plane strain,[3,9] determined by the factor K and the position $\boldsymbol{R}_{\mathrm{c}}$. Internal (movable) atoms are relaxed in the finite temperature of 300 K for 2.4 ps. After the relaxation of the internal atoms, the position $\boldsymbol{R}_{\mathrm{c}}$ is shifted by $1/10$ of one atomic increment and the relaxation is restarted. The resultant cleaved surface shows the buckled (2×1) structure, as in Fig. 2 of Ref. 9. In our simulations, the increase of the reconstructed surface area by one atomic increment occurs within the typical time scale of 0.1 ps.

The present calculations resulted in a typical value of $K_{\mathrm{prop}}=0.7$ MPa $\sqrt{\mathrm{m}}$, which agrees satisfactorily with the previous theoretical and experimental values of $0.41-1.24$ MPa $\sqrt{\mathrm{m}}$ listed in Table 1 of Ref. 9. Since the calculated surface energy in Appendix A is somewhat overestimated, for example, by approximately 40% in $\gamma_{111}^{2\times1}$, we speculate that the present value of K_{prop} is an overestimated one, owing to the limited freedom of the present Hamiltonian.[47]

---

[1] A. A. Griffith, Philos. Trans. R. Soc. London, Ser. A **221**, 163 (1920).

[2] N. F. Mott, Engineering (London) **165**, 16 (1948).

[3] As general references of brittle fracture, L. B. Freund, *Dynamic Fracture Mechanics* (Cambridge University Press, Cambridge, UK, 1989); B. Lawn, *Fracture of Brittle Solids*, 2nd ed. (Cambridge University Press, Cambridge, UK, 1993).

[4] As a review, H. Neddermeyer, Rep. Prog. Phys. **59**, 701 (1996).

[5] K. C. Pandey, Phys. Rev. Lett. **47**, 1913 (1981).

[6] J. E. Northrup and M. L. Cohen, Phys. Rev. Lett. **49**, 1349 (1982).

[7] F. Ancilotto, W. Andreoni, A. Selloni, R. Car, and M. Parrinello, Phys. Rev. Lett. **65**, 3148 (1990).

[8] Y. M. Huang, J. C. H. Spence, O. F. Sankey, and G. B. Adams, Surf. Sci. **256**, 344 (1991).

[9] J. C. H. Spence, Y. M. Huang, and O. Sankey, Acta Metall. Mater. **41**, 2815 (1993).

[10] M. Rohlfing and S. G. Louie, Phys. Rev. Lett. **83**, 856 (1999).

[11] M. Henzler, Surf. Sci. **36**, 109 (1973).

[12] M. A. Lutz, R. M. Feenstra, and J. O. Chu, Surf. Sci. **328**, 215 (1995).

[13] R. Pérez and P. Gumbsch, Phys. Rev. Lett. **84**, 5347 (2000).

[14] See the following recent work or references therein; A. A. Stekolnikov, J. Furthmüller, and F. Bechstedt, Phys. Rev. B **65**, 115318 (2002).

[15] Recent fine experimental and theoretical works discussed the difference between the (111)-(2×1) structures of Si and Ge; H. Hirayama, N. Sugihara, and K. Takayanagi, Phys. Rev. B **62**, 6900 (2000); M. Rohlfing, M. Palummo, G. Onida, and R. Del Sole, Phys. Rev. Lett. **85**, 5440 (2000).

[16] T. Hoshi and T. Fujiwara, J. Phys. Soc. Jpn. **69**, 3773 (2000).

[17] T. Hoshi and T. Fujiwara, Surf. Sci. **493**, 659 (2001).

[18] T. Hoshi and T. Fujiwara, J. Phys. Soc. Jpn. **72**, 2429 (2003).

[19] M. Geshi, T. Hoshi, and T. Fujiwara, J. Phys. Soc. Jpn. **72**, 2880 (2003).

[20] R. Takayama, T. Hoshi, and T. Fujiwara, J. Phys. Soc. Jpn. **73**, 1519 (2004).

[21] T. Hoshi, Ph.D. thesis, University of Tokyo (2003); T. Hoshi (unpublished).

[22] I. Kwon, R. Biswas, C. Z. Wang, K. M. Ho, and C. M. Soukoulis, Phys. Rev. B **49**, 7242 (1994).

[23] In a recent experiment, for example, the cleavage propagation velocity on the Si(111) plane is given as $v=2.3\pm0.3$ km/s; J. A. Hauch, D. Holland, M. P. Marder, and H. L. Swinney, Phys. Rev. Lett. **82**, 3823 (1999).

[24] The surface energy of silicon is always given on the order of $1\ \text{J/m}^2$ or 1 eV per atom.

[25] Surface energy of several *ideal* surfaces can be explained by the number of broken-bond sites per unit area. For example, the number of broken-bond sites on the (111) surface is smaller than that on the (001) surface, which explains the fact that the surface energy of the *ideal* Si(111) surface is smaller than that of the *ideal* Si(001) surface ($\gamma_{(001)}^{\text{ideal}}=2.39\ \text{J/m}^2, \gamma_{(111)}^{\text{ideal}}=1.82\ \text{J/m}^2$). (see Ref. 14). As discussed in the text, this simple explanation is not valid for the *reconstructed* silicon surfaces.

[26] Y. Mera, T. Hashizume, K. Maeda, and T. Sakurai, Ultramicroscopy **42–44**, 915 (1992).

[27] D. Haneman, Phys. Rev. **121**, 1093 (1961).

[28] R. M. Feenstra and J. A. Stroscio, Phys. Rev. Lett. **59**, 2173 (1987).

[29] H. Tokumoto, S. Wakiyama, K. Miki, H. Murakami, S. Okayama, and K. Kajimura, J. Vac. Sci. Technol. B **9**, 695 (1991); T. Komeda, S. Gwo, and H. Tokumoto, Jpn. J. Appl. Phys., Part 1 **35**, 3724 (1996).

[30] As a common tendency among tilted structures on Si or Ge surfaces, the vacuum side atom has an *excess* electron population, on the order of 0.1 e and the bulk side atom has a *deficit* population. This can be explained by the hybridization freedom; D. J. Chadi, Phys. Rev. Lett. **43**, 43 (1979). The tendency is seen in the bucked and π-bonded Si or Ge (111)-(2×1) structures (see Sec. III).

[31] D. J. Chadi and J. R. Chelikowsky, Phys. Rev. B **24**, 4892 (1981).

[32] Yutaka Mera (private communication).

[33] Masakazu Ichikawa (private communication).

[34] K. Fujita, Y. Kusumi, and M. Ichikawa, Surf. Sci. **357–358**, 490 (1996).

[35] A. A. Shklyaev and M. Ichikawa, Phys. Rev. B **65**, 045307 (2002).

[36] For example, a hybrid scheme within quantum mechanics gave a simulation of 10^5 Si atoms (see Refs. 18 and 21), in which the perturbative and variational procedures are used simultaneously in one sample.

[37] J. C. Phillips, Rev. Mod. Phys. **42**, 317 (1970).

[38] W. A. Harrison, *Electronic Structure and the Properties of Solids* (W. H. Freeman and Company, San Fransisco, 1980).

[39] P. Vogl, H. P. Hjalmarson, and J. D. Dow, J. Phys. Chem. Solids **44**, 365 (1983).

[40] O. K. Andersen, O. Jepsen, and D. Glötzel, in *Highlights of Condensed Matter Theory*, edited by F. Bassani, F. Fumi, and M. P. Tosi (North Holland, Amsterdam, 1985).

[41] O. K. Andersen, T. Saha-Dasgupta, R. W. Tank, C. Arcangeli, O. Jepsen, and G. Krier, in *Electronic Structure and Physical Properties of Solids. The Uses of the LMTO Method*, edited by H. Dreysse (Springer-Verlag, Berlin, 2000), p. 3.

[42] O. K. Andersen, T. Saha-Dasgupta, and S. Ezhov, Bull. Mater. Sci. **26**, 19 (2003).

[43] C. H. Xu, C. Z. Wang, C. T. Chan, and K. M. Ho, J. Phys.: Condens. Matter **4**, 6047 (1992).

[44] P. Krüger and J. Pollmann, Phys. Rev. Lett. **74**, 1155 (1995).

[45] C.-C. Fu, M. Weissmann, and A. Saúl, Surf. Sci. **494**, 119 (2001).

[46] S. Nosé, Mol. Phys. **52**, 255 (1984); W. G. Hoover, Phys. Rev. A **31**, 1695 (1985).

[47] In the continuum theory, the critical value of the stress intensity factor K is proportional to the square root of surface energy ($K \propto \sqrt{\gamma}$) (see Refs. 1, 3, and 9).